Nanosecond laser irradiation synthesis of CdS nanoparticles in a PVA system

Damian C. Onwudiwe[1], Tjaart P Krüger[2], Oluwafemi S. Oluwatobi[3], Christien A. Strydom*[1]

[1]Chemical Resource Beneficiation (CRB) Research Focus Area, North-West University, Private Bag X6001, Potchefstroom2520, South Africa

[2]Department of Physics, University of Pretoria, Private Bag X20, Hatfield 0028, South Africa

[3]Department of Chemistry and Chemical Technology, Walter Sisulu University, Mthatha campus Private Bag X1, Mthatha, South Africa

* Corresponding author: Prof. Christien A. Strydom

Telephone: +27 18 299 2340

Fax: +27 18 299 2350

E-mail: christien.strydom@nwu.ac.za

Research Highlights

- CdS quantum dots in PVA polymer matrices were prepared
- Nucleation and growth occurred via nanosecond laser irradiation.
- PVA effectively passivated the surface of the CdS
- CdS nanoparticles obtained are spherical and crystalline.
- Strong blue shift in the band gap was observed in the UV-vis spectra

Graphical Abstract

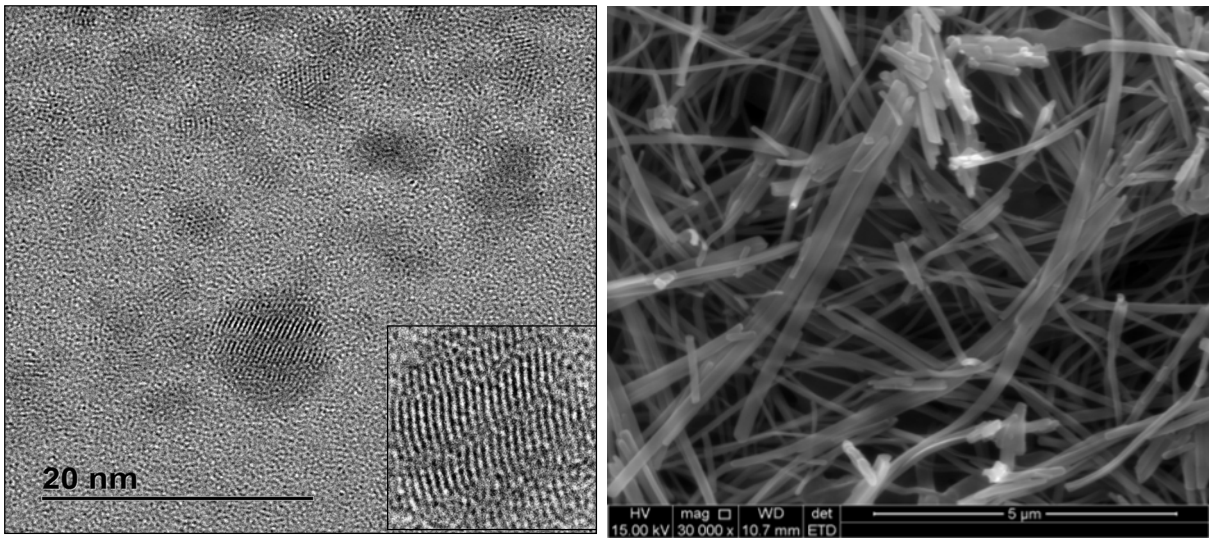

Abstract

We herein report a modified, *in situ* photolytic process for the nucleation and growth of cadmium sulphide nanoparticles in the presence of an optically transparent and semicrystalline polyvinyl alcohol (PVA) polymer matrix. The laser causes a localized decomposition of the precursor species in the immediate vicinity of the polymer leading to highly confined nanocrystals. The as-synthesised PVA-CdS nanocomposite was characterised using UV-vis absorption and photoluminescence spectroscopy, scanning electron microscopy (SEM), transmission electron microscopy (TEM), high resolution TEM (HRTEM) and powdered X-ray diffraction (XRD). Strong blue shift in the band gap was observed in the UV visible absorption spectrum indicating the size confinement. The influence of deposition temperature (25 – 200 ^{o}C) on the optical properties, microstructure, and thermal stability was also investigated. Thermal decomposition behaviour of these composites exhibit decreased thermal stability as indicated by the shift in the decomposition temperature of the pure PVA. XRD patterns revealed a reduction in the crystallinity of the polymer due to the entrapped particles. The nanocomposites showed the existence of both cubic and

hexagonal phases. The hexagonal phases dominates at lower temperature (25 and 50 ^{o}C) while the cubic phase dominates at higher temperature (100 – 200 ^{o}C).

Keywords: Nanosecond laser; CdS nanoparticles; PVA; optical properties; structural properties.

1. Introduction

The synthesis of nanometer-size clusters and particles for electronic and optical materials is at the heart of many fundamental studies in modern chemistry and materials science. This is due to the fact that at this nanosize range electronic and structural properties of a solid change dramatically [1]. The II–VI types of semiconductor nanoparticles represent ideal systems for dimension-dependent properties, and have been extensively studied for its optoelectronic, photochemical, and nonlinear optical applications [2]. Various routes widely used for the synthesis of this class of nanoparticles include physical methods such as sputtering and vapour-phase condensation, while the chemical methods involve reactions in various media, chemical precipitation [3], and thermal decomposition in coordinating solvent [4].

Laser radiation-induced decomposition of metal complexes has recently aroused research interest due to its several advantages over the conventional pyrolytic method. Laser assisted decomposition processes from organometallics have the advantages of spatial selectivity of deposition on the substrate, selective energy transfer to the deposition precursor, and low processing temperatures [5]. By selective energy transfer to the precursor molecule, the photochemical syntheses can proceed at low temperature, even close to ambient, since

photon energy rather than thermal energy is used to initiate homogeneous reactions for the production of chemically active ions and radicals that can participate in heterogeneous reactions [6]. This is one distinct advantage of photolysis over pyrolysis.

The nanometer-size particles, due to their reduced size, possess a high fraction of surface atoms with the surface atom fraction decreasing gradually as the particle size increases [7]. The surface layers of atoms are highly reactive and tend to agglomerate producing larger crystallites or migrate to interfacial regions; consequently, the advantages of their nanoscale dimensions and unique properties are lost. One way to alleviate this challenge is by entrapping the nanoparticles in confined matrices. Polymers have been shown to be excellent hosts for trapping nanoparticles of metals and semiconductors, and also capable of acting as stabilizers or surface capping agents. When nanoparticles are embedded or encapsulated in a polymer, the polymer controls the growth rate of the particles by controlling the nucleation [8], and the resulting new class of functional materials (nanocomposites) may afford potential applications in molecular electronics, optics, photoelectrochemical cells, solvent-free coatings, etc [9]. Polymeric materials embedded with nanoparticles have high homogeneity, high processability and tunable optical properties [10 - 14]. Various approaches have been employed to prepare CdS embedded within polymeric materials. Saikia *et al* has reported the preparation of CdS/PVA nanocomposite thin films by in situ thermolysis of cadmium acetate/thiourea dispersed in polyvinyl alcohol (PVA) [15]. Incorporation of CdS nanoparticles into polymer-blend membranes of poly(styrenephosphonate diethyl ester) (PSP) and cellulose acetate (CA) has been reported. [16]. Kanade *et al* reported CdS nanoparticles embedded in polyethylene sulphide (PES) matrix by a novel polymer inorganic solid state reaction in which the

polymer serves a dual purpose of being a sulphur precursor and a capping/stabilizing agent for the prepared CdS nanoparticles [17]. A simple approach which makes use of the unique microstructure formed in the network due to the clustering of ionic groups such as SO_3 upon sulphonation has been employed to incorporate CdS nanoparticles into a polystyrene (PS) network [12]. CdS nanocrystallites with good luminescence were synthesized at high temperature in a non-coordinating solvent and doped into micrometer-size polystyrene beads generated via a suspension polymerization reaction [18]. Interestingly, Pulsed laser irradiation has been demonstrated as a possible method for the formation of metal sulphide nanoparticles directly into the well-confined area of a polymer matrix without inducing any macroscopic damage to the host matrix [19].

In this work, we report an incorporation of cadmium dithiocarbamate precursors into a polymer substrate and subsequent *in situ* nucleation of cadmium sulphide nanoparticles directly into the polymer matrices by nanosecond laser irradiation, hence resulting in polymer-encapsulated nanoparticles. Additionally, we studied how the properties of the nanoparticles are affected by temperature as an important thermodynamic parameter.

2 EXPERIMENTAL

2.1 Precursor-polymer preparation

The precursor compound, bis(N-ethyl-N-phenyl dithiocarbamate) Cd(II) was synthesized and added to the polymer PVA. The detailed synthesis and characterization of the precursor compound, represented as CdL_2, is described in [20]. The chemical formula for the preparation is represented as

$CdCl_2 + 2L \longrightarrow CdL_2$

Where L = N-ethyl-N-phenyl dithiocarbamate

0.20 g of the precursor compound in 10 mL of chloroform was sonicated for 30 min to obtain maximum dispersion. This solution was then added to PVA solution containing 0.8 g of PVA in 10 mL of toluene and stirred at 60 ^{o}C for 4 h. The solution was finally casted on glass slides to produce the film after evaporation of the solvents. The dried films were slowly heated at 80 ^{o}C for six hours to remove any entrapped solvent.

2.2 Thin Film Preparation

The microscope glass slides were cleaned by rinsing in diluted HCl, and then sonicated in soap for 10 min, followed by flooding with distilled water. Finally, they were rinsed in acetone and dried in the oven overnight. The casting of the substrate on the glass slides were carried out manually.

2.3 Preparation of Nanoparticles

The nanocrystals in the polymer matrices were formed by irradiating the samples with short, high-intensity laser pulses. Third-harmonic pulses at 355 nm from an Nd:YAG Q-switched nanosecond laser (EKSPLA NT342B-SH-10-AW) were used. The pulse repetition rate was 10 Hz, while the pulse length and the pulse duration were <0.13 nm and ~4 ns respectively. The energy per pulse emanating from the laser source was determined as 110.0 ± 2.6 mJ and decreased by 15-16 % before reaching the sample. During photolysis, the substrate temperature was varied from room temperature (25 ^{o}C) to 200 ^{o}C. The samples,

irradiated with the same pulses of energy (110 mJ) for 10 min, were denoted as S_X, where X = 25, 50, 100, 150, and 200, representing substrate temperatures in ^{o}C.

Fig. 1 shows a schematic diagram of the apparatus constructed to carry out the laser induced decomposition. The samples were positioned in the center of the reactor cell using microscope glass slides with dimensions 76 mm × 26 mm × 1 mm (LASEC). They were preheated on a heating stage using an electrical heater to a specific temperature between 25 and 200 °C. After 10 min of heating at a specific temperature, allowing the entire substrate to attain a uniform temperature, the laser beam was introduced into the chamber through a quartz window at an angle of ∼51° with respect to the substrate normal and was expanded by a plano-concave lens (CVI Melles Griot) to a diameter of ∼20 mm at the substrate surface. The laser intensity profile on the substrate surface is displayed in the Supplementary Figure S1.

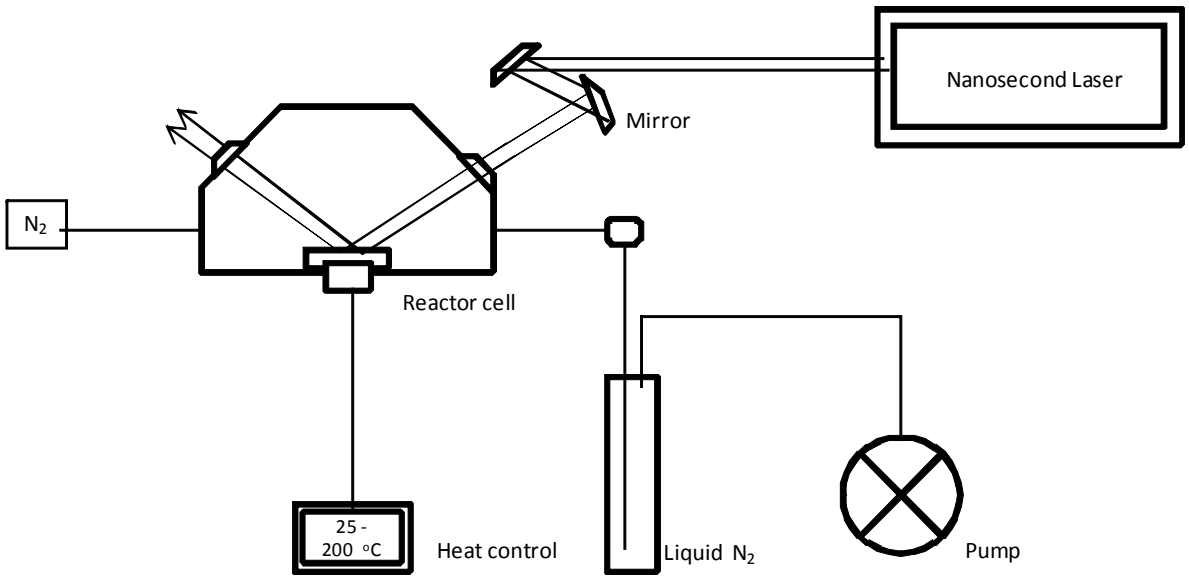

Figure 1 schematic diagram of the Laser set-up

2.4. Sample characterizations

The absorption measurements were carried out using a PerkinElmer Lambda 20 UV–vis spectrophotometer at room temperature. A PerkinElmer LS 55 luminescence spectrometer was used to measure the photoluminescence of the nanoparticles.

Scanning electron microscopy (SEM, a Quanta FEG 250 Environmental Scanning electron microscope (ESEM)) was used to investigate the surface morphology of the nanocomposite. A thin gold layer was deposited to improve the electrical conductivity for better imaging.

High resolution TEM images were taken using a JEOL 2100 HRTEM, fitted with a LaB_6 electron gun. Samples were suspended in DMSO, sonicated for 1 min and dispersed on carbon-coated grids. Analysis was done at 200 kV, and images were capture using a Gatan Ultrascan digital camera.

Powder X-ray diffraction was used to confirm the crystalline phases for each sample. The X-ray powder diffraction data were collected on a Röntgen PW3040/60 X'Pert Pro X-ray diffractometer using Ni-filtered Cu Kα radiation (λ= 1.5405 A) at room temperature. X'Pert HighScore Plus PW3212 software was used for the analysis and the phase identification was carried out with using standard JCPDS.

Thermal analysis (TGA, a SDTQ 600 Thermal instrument) was conducted from room temperature to 650 ^{o}C under flowing nitrogen using the simultaneous thermal analysis (STA) technique for parallel recording of TG (thermogravimetry) and DSC (differential scanning calorimetry) curves. A heating rate of 10 °C min^{-1} was used.

3. Results and discussion

3.1. Preparation of the PVA-CdS layers

Figure 1 shows a schematic diagram of the apparatus constructed to carry out the laser induced decomposition. The samples were positioned in the center of the reactor cell using microscope glass slides with dimensions 76 mm x 26 mm x 1 mm (LASEC). They were preheated on a heating stage using an electrical heater to a specific temperature between 25 and 200 ^{o}C. After 10 min of heating at a specific temperature, allowing the entire substrate to attain an uniform temperature, the laser beam was introduced into the chamber through a quartz window at an angle of ~51° with respect to the substrate normal and was expanded by a plano-concave lens (CVI Melles Griot) to a diameter of ~20 mm at the substrate surface. The laser intensity profile on the substrate surface is displayed in the Supplementary Figure S1.

Polyvinyl alcohol (PVA, MW = 88000 – 96800) was used as the polymer nanocomposite matrix and the stabilizer to prevent nanoparticle agglomeration. A layer of a polymer and CdS were prepared using an *in-situ*-photolytic formation process by irradiating the metal complex entrapped directly within the matrices of the polymer. The polymer (PVA) contains polar side groups, which is necessary to ensure a homogeneous precursor solution of the polymer and the inorganic compound. The precursor to polymer ratio was chosen so that complete decomposition of the metal complex would yield CdS which is well passivated by the polymer molecule. The color of the irradiated area became light yellow, and served as an indicator for CdS nanoparticles synthesis. (See Figure S2).

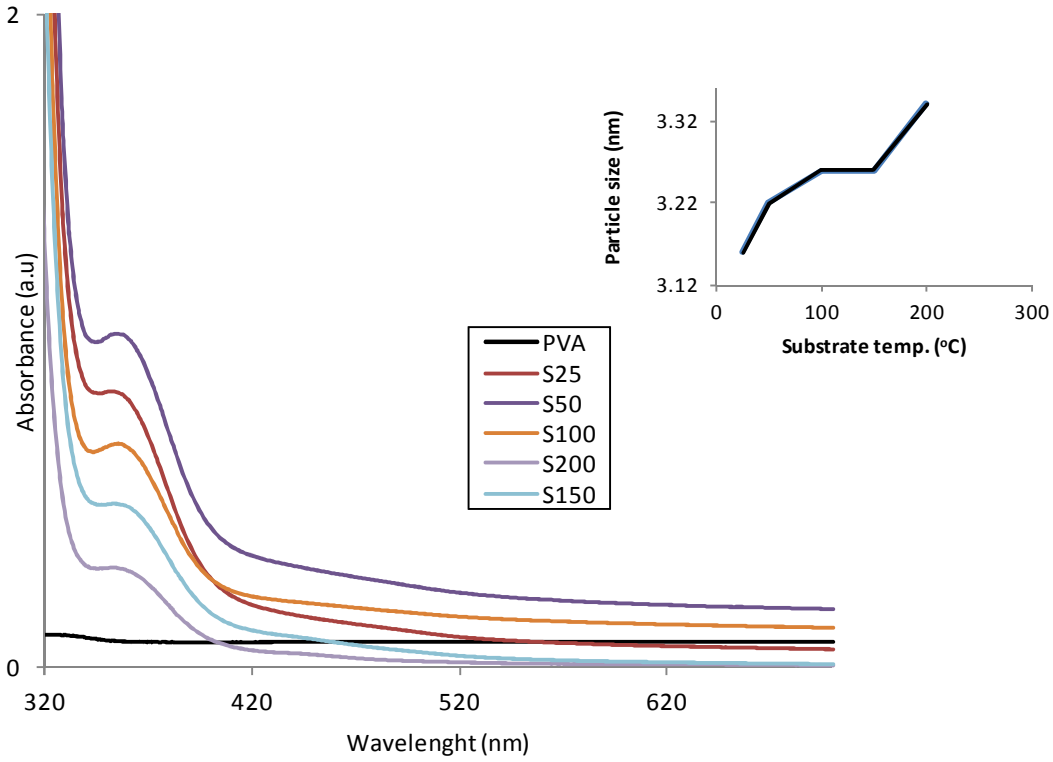

Figure 2 Absorption spectra of pure PVA and CdS/PVA nanocomposite film at different substrate temperatures.

3.2 Optical Properties

The absorption spectra of the as-synthesised CdS nanoparticles as a function of substrate temperature are shown in Figure 2. Pure PVA was found to show no absorption within the measured range (300 – 700 nm); hence, the absorption between 300 and 700 nm has been attributed to the CdS nanoparticles embedded within the matrices of the PVA. In semiconductor nanoparticles, it is known that the UV/vis onset absorption is attributed to the band gap absorption, and this will be blue-shifted relative to the bulk band gap due to quantum size confinement effect [21, 22]. The absorption spectra of all the samples are greatly blue-shifted relative to bulk CdS at 512 nm, indicating the formation of nanometer-sized CdS particles. The absorption spectrum of the sample prepared at room temperature (S25) shows absorption onset at about 398 nm, with a shoulder (characteristic of cadmium

suphide nanoparticle) around 356 nm. As the temperature increased, a slight shift in the absorption onset towards red is observed indicating increase in particle size. This result is in agreement with previously reported data for colloidal CdS prepared in the presence of PVA where positions of absorption peaks were found to be between 320 and 390 nm [23]. The band gap energy was estimated from the cut-off wavelength of the intersection of the tangent line of the peak with the wavelength axis using the relationship:

$$E^{*} = \frac{hc}{\lambda_c} \quad \text{..... (1)}$$

Where λ_c = wavelenght of light absorbed by the sample and c is the speed of light.

Table 1. Variation of size at different substrate temperatures

Substrate temp. (^{o}C)	Critical absorption wavelength(λ) (nm)	Band gap energy (eV)	Energy stoke shift (eV)	Particle size (nm)
25	398	3.12	0.70	3.16 ± 0.06
50	402	3.08	0.66	3.22 ± 0.04
100	405	3.06	0.64	3.26 ± 0.04
150	405	3.06	0.64	3.26 ± 0.05
200	410	3.02	0.60	3.34 ± 0.05

The particle diameter (*D*) was calculated from the shift in the band gap energy using the effective mass approximation [24], (equation 2.0), and presented in Table 1.

$$\Delta E_g = E_g^{nano} - E_g^{bulk} = \frac{h^2}{8r^2}\left(\frac{1}{m_e^*} + \frac{1}{m_h^*}\right) - \frac{1.8e^2}{4\pi\varepsilon\varepsilon_o r} \quad \text{..... (2.0)}$$

where r is the particle radius, E_g^{nano} and E_g^{bulk} are the energy gaps of nano and bulk materials, respectively, and m_e^* and m_h^* are the effective masses of an electron and a hole in the bulk CdS (CdS m^*/m_e = 0.2). ε is the dielectric constant and it is 5.6. The size and morphology of nanoparticles do not only depend on the chemical composition of the starting solution but also depends on the method and conditions of synthesis. The results show that laser breakdown in the presence of a capping group is an effective way to prepare stable nanoparticles of very small size. The particles sizes as calculated are between 3.16 + 0.06 nm to 3.34 + 0.05 nm as the substrate temperature increases. The inset in Figure 2 illustrates the change in particle size with substrate temperature. The graph shows that increase in temperature has little effect or does not greatly enhance particle growth until the decomposition temperature of the PVA is approached.

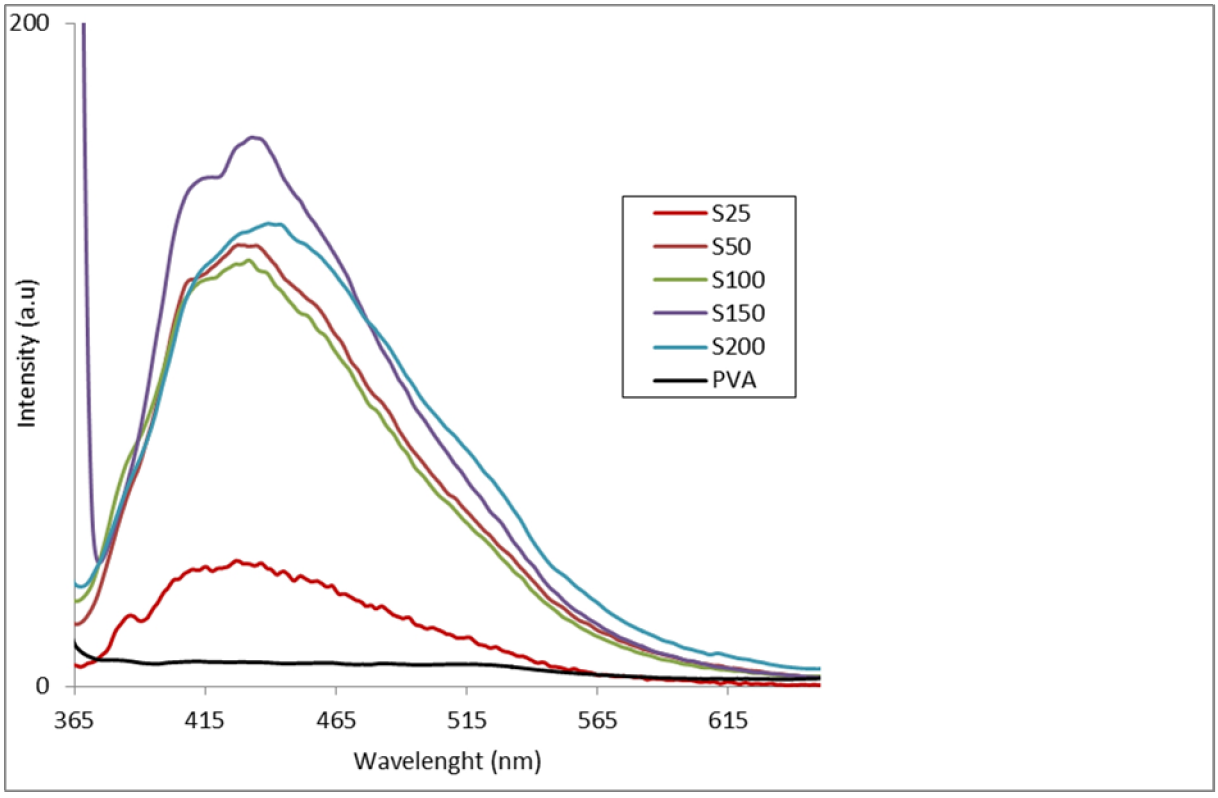

Figure 3. Fluorescence spectra of PVA thin film and PVA-CdS composite at different substrate temperatures

In the nanometer size regime, quantum confinement effects affect most notably the electronic properties of the particle [23]. CdS nanoparticles are known to exhibit light-emitting behaviour at a specific wavelength [25 – 29]. Thus, the formation of CdS nanoparticles can also be confirmed by photoluminescence (PL) spectroscopy. Figure 3 shows the photoluminescence spectra of the PVA and PVA capped CdS nanoparticles at the excitation wavelength of 370 nm. This emission peak is assigned to the electron-hole recombination of CdS [22]. The spectra show a broad luminescence at 425 nm for the sample obtained at room temperature, S25. The enhanced luminescence intensity of the polymer-capped CdS nanoparticles as the temperature increased is ascribed to the surface modification by PVA molecules. The PVA as a capping agent minimized the surface defects and enhanced the possibility of electron-hole recombination. There was no fluorescence for the pure PVA sample in the observed wavelength range from 365 nm to 650 nm [30]. The spectra for samples Sx (X = 50, 100, 150 and 200) exhibited emission maximum peaks at about 430 nm.

3.3 Structural Properties

The SEM images of the PVA-CdS nanocomposites at different substrate temperatures are shown in figure 4. The micrographs show that the microstructures of these composites are quite similar except for a small increase in particle aggregation. The structural aggregation appears to be either side-by-side or head-to-head/head-to-tail as the temperature increases with an increase in the grain size. It is possible that as the growth temperature increased, an increase in entropy is facilitated. Accordingly, the number of bonds between the −OH ions and the nanocrystals in the substrate solution are reduced, and more nanocrystals are able

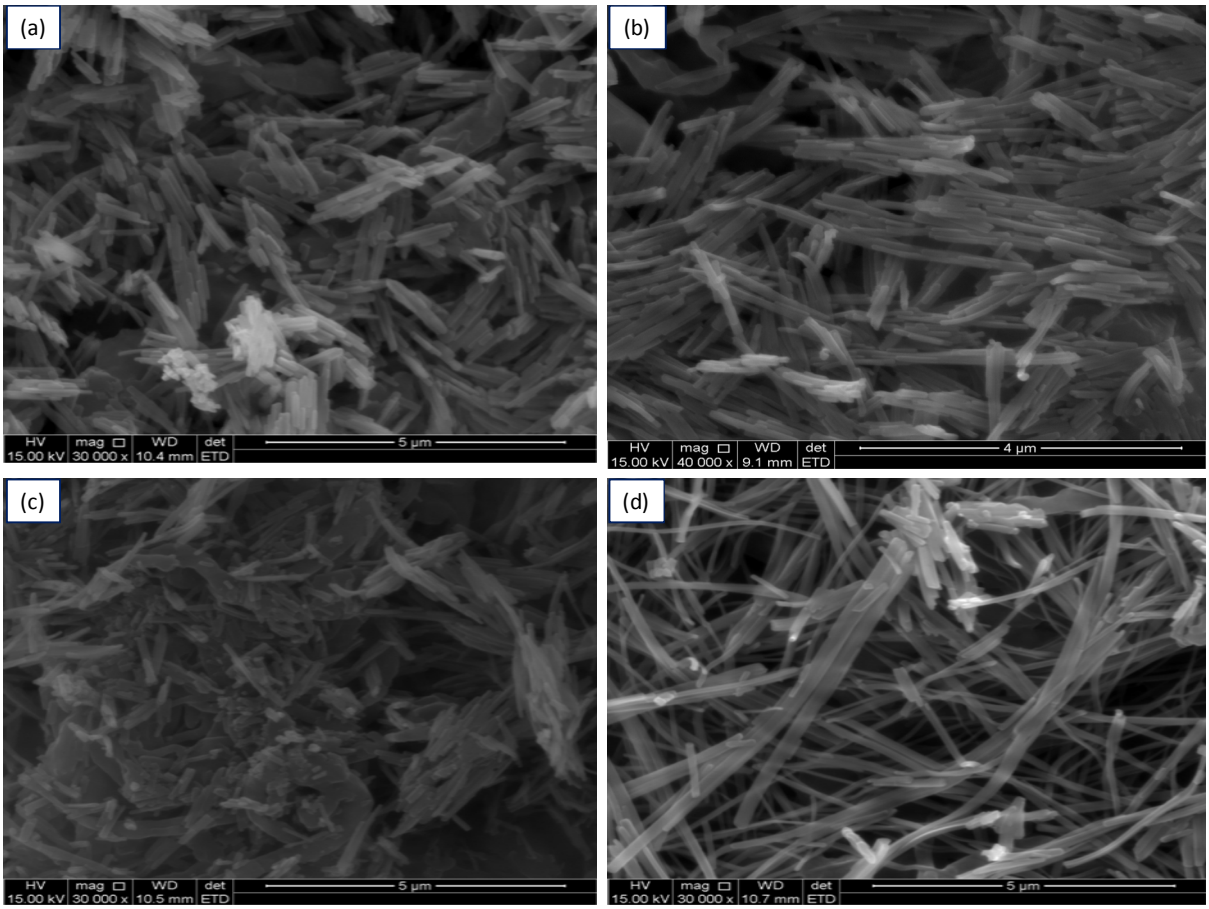

Figure 4. Surface SEM images of PVA-CdS nanocomposites prepared at substrate temperatures of (a) 25, (b) 50, (c) 150 and (d) 200 ^{o}C

to interact with one another. Hence, the aggregation of particles increased at high temperatures. In addition the long-axis length of the composites also increased.

Figure 5(a)–(c) show the TEM images of the PVA-CdS at different substrate temperatures. Figure 5(a) shows that the CdS exists in the PVA matrix as dispersed nanoparticles. The particles are spherical, monodispersed and loosely distributed with an average particle diameter of 4.5 nm. As the temperature increased the size of the PVA-capped nanoparticles also increased in accordance with the optical analyses. The high resolution TEM images (Fig. 5(b) and (c)) show that the particles are spherical and highly crystalline as confirmed by the

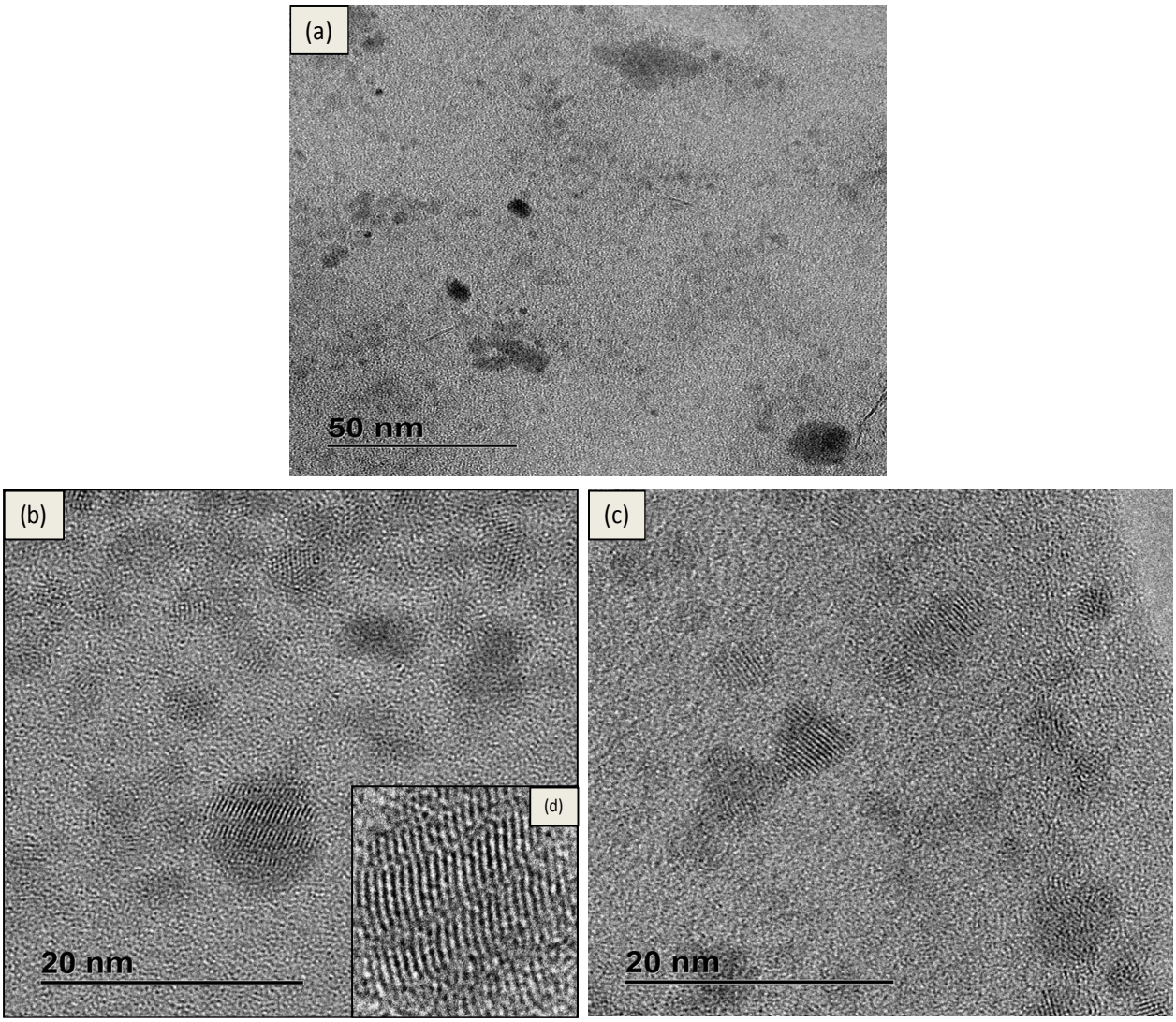

Figure 5. TEM micrographs of the PVA containing CdS nanoparticles, prepared at different substrate temperatures of (a) 25 ^{o}C, (b) 50 ^{o}C (inset shows the presence of lattice fringes) and (c) 100 ^{o}C.

presence of lattice fringes. At higher temperatures (150 and 200 ^{o}C), Figure 6, some degrees of agglomeration becomes visible. At 200 ^{o}C, (Fig 6(b)), the particles lattice fringes are almost invisible, and size determination becomes almost non-feasible due to fuzzy particle boundary.

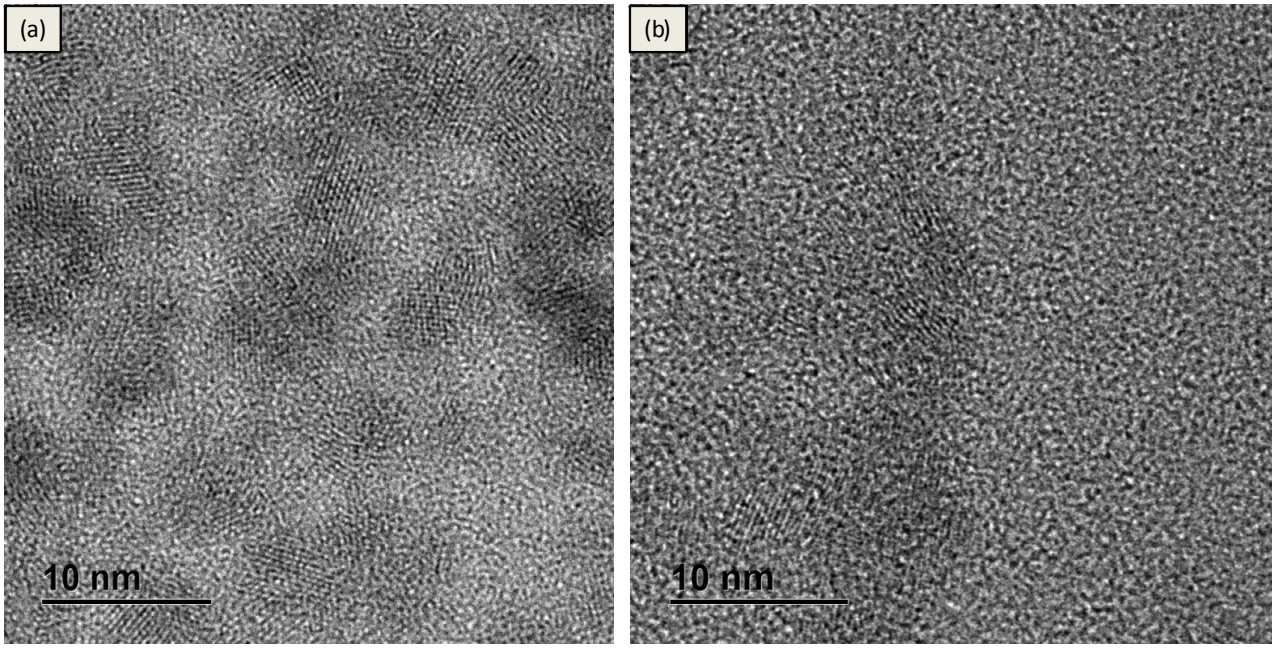

Figure 6. TEM micrographs of the PVA containing CdS nanoparticles, prepared at different substrate temperatures of (a) 150 ^{o}C and (b) 200 ^{o}C.

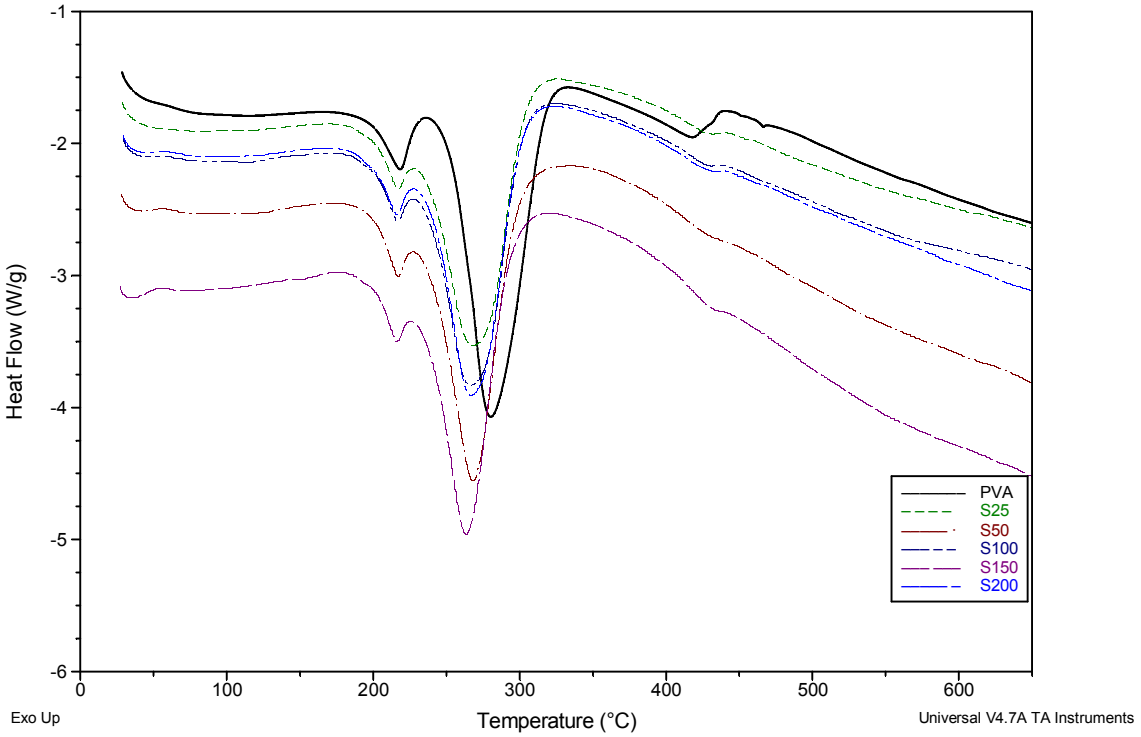

Figure 7. DSC thermogram of pure PVA and nanocomposite at different substrate temperatures. Heating rate = 10 ^{o}C min^{-1}

3.4 Thermal properties

The thermal stability and degradation behavior of PVA and the CdS-PVA nanocomposites were investigated using TGA-DSC under nitrogen flow. The resulting thermograms are shown in Figures 7 (a) and (b). The PVA was found to be highly crystalline with a crystalline melting point, T_m, of ~218 °C. The figure showed no change in the melting temperature for both pure polymer and the nanocomposite. A glass transition was not observed. This result indicates that the presence of CdS nanoparticles do not lead to a decrease in the overall lamellar size of the PVA. However, the presence of CdS caused a decrease in the decomposition temperature of the PVA by ~20 °C. This confirms a strong interaction between PVA and CdS. It is known that the crystalline nature of PVA results from the strong intermolecular interaction between PVA chains through the intermolecular hydrogen bonding [31]. Thus, it is possible that in our study the interactions between PVA chains and CdS particles led to the decrease of intermolecular interaction between the PVA chains and thus the crystalline degree [32].

Non-isothermal TG of the pure PVA and the nanocomposites were carried out at a heating rate of 10 °C min^{-1}. The results are shown in Figure 8 for the pure PVA and PVA-CdS nanocomposite films at different substrate temperature, Sx (x = 25, 50, 100, 150, and 200 ^{o}C). The thermal decomposition of the samples fits a two-stage phenomenon (~240 – 330 °C and 350 – 480 °C) [33]. The bulk of the weight loss took place between 200 and 300 °C, followed by a further weight loss between 350 and 450 °C. The residues left after the thermal decomposition are greater in PVA-CdS compared to the pure polymer, and the difference could be attributed to the CdS nanoparticles content. The results were consistent with the elimination of side-groups at lower temperatures, followed by breakdown of the

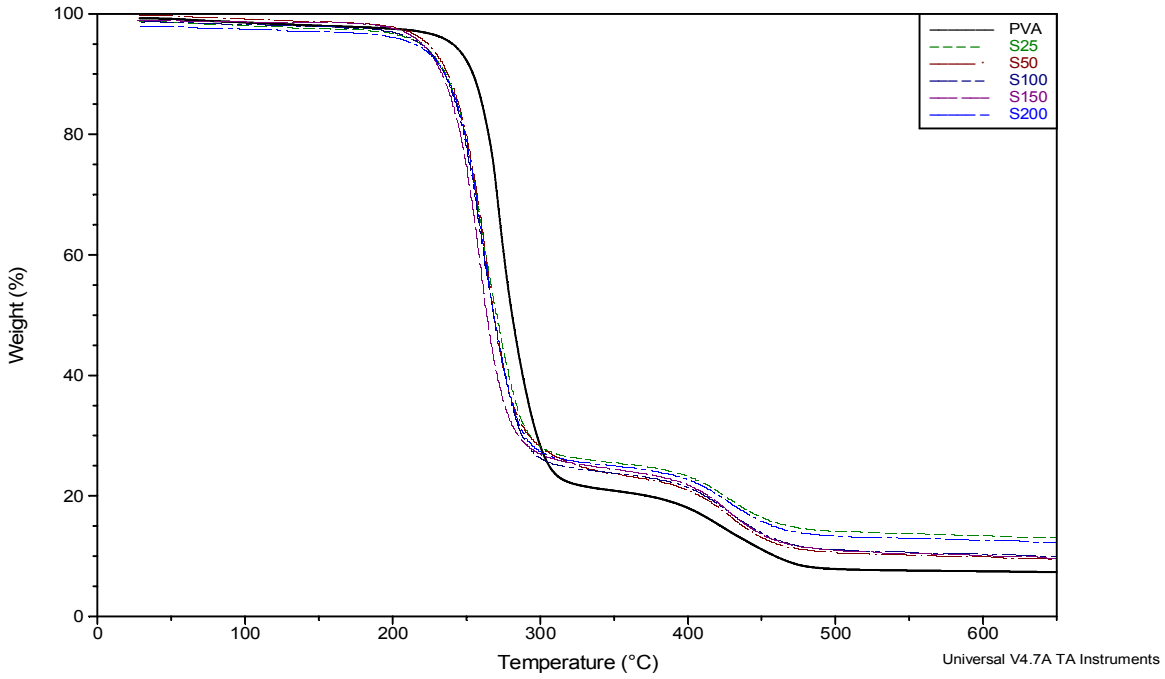

Figure 8. Non-isothermal TG of pure PVA and nanocomposite at different substrate temperatures. Heating rate = 10 ^{o}C min^{-1}

polymer backbone at higher temperatures [34]. From the graphs, the thermal decomposition temperature of the PVA- CdS nanocomposite film was lowered by about 25 ^{o}C compared to pure PVA film. The lowering of the decomposition temperature has been attributed to the interactions between PVA and CdS. Such interaction could lead to decrease in the intermolecular interaction between the PVA chains and the crystalline degree, thus lowering the thermal stability of PVA -capped CdS nanoparticles.

Different types of nanofillers have been found to have different influences on the thermal stability of a PVA matrix. For example, while 50 Å Ag nanoparticles improved the thermal stability of the PVA matrix by about 40 $^{\circ}$C, the thermal decomposition of the PVA is unchanged in the presence of montmorillonite. On the other hand, in the presence of the magnetite nanoparticles, decomposition of the PVA is shifted towards lower temperatures

by approximately 20 °C [35]. Lowering of the thermal stability of polymer in the presence of CdS nanoparticles had also been reported by Kuljanin-Jakovljević et al.,[36]. In their report, polystyrene (PS) was used as the polymer with PS-CdS ratio of 80/20. The low stability was attributed to the concentration of the CdS nanoparticles.

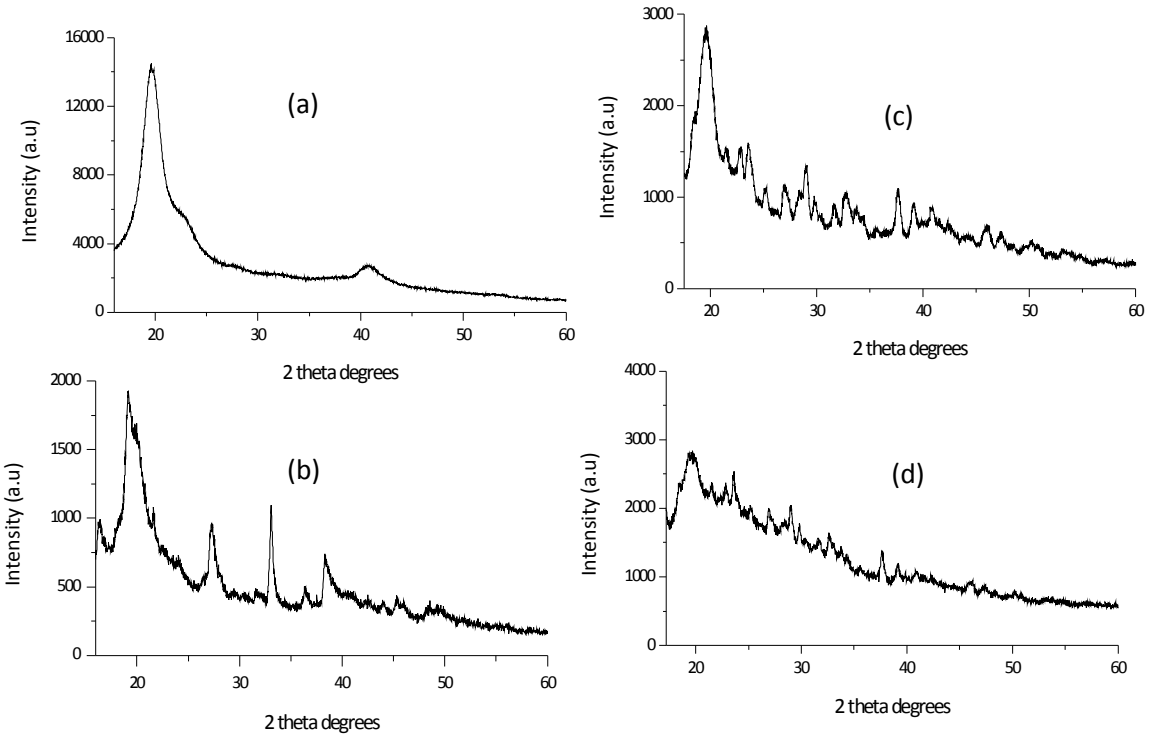

Figure 9. XRD patterns of (a) pure PVA, (b) PVA + CdL_2 (before irradiation), (c) PVA+CdL_2 (after irradiation 25 ^oC, S25), and (d) PVA+CdL_2 (after irradiation at 150 ^oC, S150)

3.4 X-ray diffraction studies

Figure 9 presents the X-ray diffraction patterns of (a) PVA, (b) PVA-CdL_2 (before laser irradiation), and PVA-CdL_2 (after laser irradiation) at substrate temperature of (c) 25 ^oC, and (d) 150 ^oC. All the spectra showed three peaks at around $2\theta = 20$, 23 and 40.4°, indicating the semi crystalline nature of PVA, which contains crystalline and amorphous domains in the matrix [37]. After the reaction of PVA with the complex (CdL_2), the intensity of the PVA diffraction peaks decreased (b). This has been attributed to the interactions between PVA

and the complex which lead to a decrease in the intermolecular interaction between the PVA chains and thus the crystalline degree [38]. Upon nanosecond laser irradiation (Figure 9(c) and (d)), a shift to a higher value of 2θ = 22.85 ^{o} was observed. The diffraction peaks of PVA-CdL_2 (before laser irradiation) showed peaks which are due to the entrapped complex. It is well documented that bulk CdS has stable wurtzite phases at room temperature [39], however the possibility of the crystallites occurring in either the cubic or hexagonal phases,

Table 2: The relevant data from the XRD pattern of the prepared sample S25

Pos. [°2Th.]	**d-spacing [Å]**	**h**	**k**	**l**	**Assignment**
20.7485	4.28823	0	1	1	h-CdS (04-006-0809)
23.0193	3.87011	0	2	1	c-CdS (04-004-1000)
26.1414	3.41456	1	1	2	c-CdS (04-004-1000)
29.7202	3.01105	0	1	2	h-CdS (04-006-0809)
36.7968	2.44057	1	1	0	h-CdS (04-006-0809)
39.1382	2.3055		1	1	3 c-CdS (04-004-1000)
41.6639	2.1714		0	1	3 h-CdS (04-006-0809)
43.6081	2.07901	0	2	3	c-CdS (04-004-1000)
44.486	2.0400		0	2	0 h-CdS (04-006-0809)
45.4924	1.99224	1	1	2	h-CdS (04-006-0809)
45.5971	1.98791	1	2	3	c-CdS (04-004-1000)
45.6382	1.99115	1	1	2	h-CdS (04-006-0809)
46.5426	1.95455	0	2	1	h-CdS (04-006-0809)
48.8444	1.86307	0	0	4	h-CdS (04-006-0809)
51.6762	1.76743	0	4	1	c-CdS (04-004-1000)
52.4349	1.74796	0	2	2	h-CdS (04-006-0809)
53.7918	1.70704	1	1	4	c-CdS (04-004-1000)
55.3945	1.65727	0	1	4	h-CdS (04-006-0809)
55.5729	1.65648	0	1	4	h-CdS (04-006-0809)

Table 3: The relevant data from the XRD pattern of the prepared sample S150

Pos. [°2Th.]	d-spacing [Å]	h	k	l	Assignment
26.8985	3.31192	1	1	1	c-CdS (04-006-2805)
27.3907	3.2616	0	0	2	h-CdS (04-003-2268)
28.5205	3.13492	1	1	1	h-CdS (04-006-2805)
33.0543	2.71457	0	0	2	c-CdS (04-006-2805)
37.7016	2.38998	0	1	2	h-CdS (04-003-2268)
44.6624	2.02732	0	2	2	c-CdS (04-006-2805)
44.76	2.02815	1	1	0	h-CdS (04-003-2268)
44.7794	2.02731	2	2	0	c-CdS (04-006-2805)
47.3319	1.91901	0	2	2	c-CdS (04-006-2805)
49.2619	1.84825	1	0	3	h-CdS (04-003-2268)
52.9216	1.72873	3	1	1	c-CdS (04-006-2805)
54.0321	1.6958	0	2	1	h-CdS (04-003-2268)
55.4736	1.6551	2	2	2	c-CdS (04-006-2805)
56.1636	1.63639	1	1	3	c-CdS (04-006-2805)
56.4046	1.62996	0	0	4	h-CdS (04-003-2268)
58.9014	1.56668	2	2	2	c-CdS (04-006-2805)
59.0624	1.56668	2	2	2	c-CdS (04-006-2805)
62.8014	1.47844	0	1	4	h-CdS (04-003-2268)

Note: c – cubic phase, h – hexagonal phase

or a combination of both, exists. In our case, after the irradiation, the crystalline nature of the nanoparticles dominates, which becomes responsible for the evolution of the new peaks identified as CdS. The smaller size of the nanocrystals complicates the assignment of a specific phase, and it becomes difficult to exclusively assign a particular phase to each sample [40]. The relevant XRD data are presented in Table 2 and 3 for S25 (samples at lower temperatures) and S150 (for samples at higher temperatures) respectively. The XRD pattern

of the S25 sample reveals the presence of cubic and hexagonal CdS, with the hexagonal being the dominant phase. At elevated temperature, S150, the crystal phases of the sample were influenced thermodynamically and the sample showed the predominance of 111, 220 and 311 planes of the cubic phase over the hexagonal phase. The peaks from the cubic phase correspond to JCPDS no 04-006-2805.

4. Conclusion

We have successfully designed a facile solid state route to produce CdS quantum dots in PVA polymer matrices via nanosecond laser irradiation. At room temperature, PVA effectively passivated the surface of the CdS and thus restricted the oriented attachment growth and aggregation. Strong blue shift in the band gap was observed in the absorption spectra indicating the size confinement and discrete nature of energy bands. The embedded CdS nanoparticles are spherical and crystalline. It was found that the substrate temperature obviously influences the size, but has no effects on the shape of the final nanoparticle. TGA results showed that the formation of nanoparticles within the matrices results in the breakdown of strong intermolecular interaction between PVA chains, which existed through the intermolecular hydrogen bonding.

Acknowledgment

The financial support of the National Research Foundation (NRF), South Africa, and North West University, Potchefstroom, South Africa are gratefully acknowledged. The authors are grateful to James Wesley-Smith of the National Centre for Nanostructured Materials, CSIR South Africa for TEM analyses.

References

[1] R.V. Tal'roze, G.A. Shandryuk, A.S. Merekalov, A.M. Shatalova, O.A. Otmakhova, Alignment of nanoparticles in polymer matrices, Polymer Science, Ser. A, 51 (2009) 1194–1203.

[2] D.C. Onwudiwe, P.A. Ajibade, Zn(II), Cd(II) and Hg(II) complexes of N-methyl-N-phenyl dithiocarbamate as single-source precursors for the synthesis of metal sulfide nanoparticles, Mater. Lett. 65 (2011) 3258–3261.

[3] W. Chen, Z. Liu, Z.Wang, Some new observation on the formation and optical properties of CdS clusters In zeolite-y, Solid State Commun. 100 (1996)101 - 104.

[4] C.B. Murray, C.R. Kagan M.G. Bawendi, Synthesis and characterization of Monodisperse nanocrystals and Close-packed nanocrystal assemblies, Annu. Rev. Mater. Sci. 30 (2000) 545–610.

[5] J. Cheon, D.S. Talaga, J.I. Zink, Photochemical Deposition of ZnS from the Gas Phase and Simultaneous Luminescence Detection of Photofragments from a Single-Source Precursor, $Zn(S_2COCHMe_2)_2$, J. Am. Chem. Soc. 119 (1997) 163-168.

[6] J. Cheon, J.I. Zink, Gas Phase Photochemical Synthesis of II/VI Metal Sulfide Films and in Situ Luminescence Spectroscopic Identification of Photofragments, J. Am. Chem. Soc. 119 (1997) 3838-3839.

[7] D. Fan, M. Afzaal, M. A. Mallik, C. Q. Nguyen, P. O'Brien, P. J. Thomas, Using coordination chemistry to develop new routes to semiconductor and other materials, Coord. Chem. Rev. 251 (2007) 1878–1888.

[8] L.C. Courrol, F.R. de Oliveira Silva, L. Gomes, A simple method to synthesize silver nanoparticles by photo-reduction, Colloids Surf. A: Physicochem. Eng. Aspects 305 (2007) 54–57.

[9] M. Antonietti, C. Goltner, Superstructures of Functional Colloids: Chemistry on the Nanometer Scale, Angew. Chem., Int. Ed. Engl. 36 (1997) 911 - 928.

[10] Z. Guo, L.L. Henry, V. Palshin, E.J. Podlah, Synthesis of poly(methyl methacrylate) stabilized colloidal zero-valence metallic nanoparticles, J. Mater. Chem. 16 (2006) 1772 –1777.

[11] M.K. Corbierre, N.S. Cameron, M. Sutton, S.G.J. Mochrie, L.B. Lurio, A. Ruehm, R.B. Lennox, Polymer-Stabilized Gold Nanoparticles and Their Incorporation into Polymer Matrices, J. Am. Chem. Soc. 123 (2001) 10411 - 10412.

[12] H. Du, G.Q. Xu, W.S. Chin, L. Huang, W. Ji, Synthesis, Characterization, and Nonlinear Optical Properties of Hybridized CdS-Polystyrene Nanocomposites, Chem. Mater. 14 (2002) 4473 - 4479.

[13] R.L. McCarley, B. Vaidya, S. Wei, A.F. Smith, A.B. Patel, J. Feng, M.C. Murphy, S.A. Soper, Resist-Free Patterning of Surface Architectures in Polymer-Based Microanalytical Devices, J. Am. Chem. Soc. 127 (2005) 842 - 843.

[14] S. Wei, B. Vaidya, A.B. Patel, S.A. Soper, R.L. McCarley, Photochemically Patterned Poly(methyl methacrylate) Surfaces Used in the Fabrication of Microanalytical Devices, J. Phys. Chem. B 109 (2005) 16988 - 16996.

[15] D. Saikiaa, P.K. Saikia, P.K. Gogoi, M.R. Das, P. Sengupta, M.V. Shelke, Synthesis and characterization of CdS/PVA nanocomposite thin films from a complexing agent free system,

Mater. Chem. Phys. 131 (2011) 223–229.

[16] Y. Yuan, J.H. Fendler, I. Cabasso, Photoelectron Transfer Mediated by Size-Quantized CdS Particles in Polymer-Blend Membranes, Chem. Mater. 4 (1992) 312 - 318.

[17] K.G. Kanade, R.R. Hawaldar, R. Pasricha, S. Radhakrishan, T. Seth, U.P. Mulik, B.B. Kale, D.P. Amalnerkar, Novel polymer-inorganic solid-state reaction for the synthesis of CdS nanocrystallites, Mater. Lett. 59 (2005) 554 - 559.

[18] Y. Li, E.C.Y. Liu, N. Pickett, P.J. Skabara, S.S. Cummins, S. Ryley, A. J. Sutherland, P. O'Brien, Synthesis and characterization of CdS quantum dots in polystyrene microbeads, J. Mater. Chem. 15 (2005) 1238–1243.

[19] A. Athanassiou, R. Cingolani, E. Tsiranidou, C. Fotakis, A.M. Laera, E. Piscopiello, L. Tapfer, Photon-induced formation of CdS nanocrystals in selected areas of polymer matrices, Appl. Phys. Lett. 91 (2007) 153108- 153111.

[20] D.C. Onwudiwe, P.A. Ajibade, Synthesis and characterization of metal complexes of N-alkyl-N-phenyl dithiocarbamates, Polyhedron 29 (2010) 1431-1436.

[21] C.N.R. Rao, G.U. Kulkarni, P.J. Thomas, P.P. Edwards, Size-Dependent Chemistry: Properties of Nanocrystals, Chemistry-A European J. 8 (2002) 28-35.

[22] T.S. Ahmadi, Z.L. Wang, T.C. Green, A. Henglein, M.A. El-Sayed, Shape-Controlled Synthesis of Colloidal Platinum Nanoparticles, Science 272 (1996) 1924-1925.

[23] H. Wang, P. Fang, Z. Chen, S. Wang, Synthesis and characterization of CdS/PVA nanocomposite films, Appl. Surf. Scie. 253 (2007) 8495–8499.

[24] Y. Kayanuma, Quantum-size effects of interacting electrons and holes in semiconductor microcrystals with spherical shape, Phys. Rev B 38 (1988) 9797 - 9805.

[25] R.S. Kane, R.E. Cohen, R. Silbey, Semiconductor Nanocluster Growth within Polymer Films, Langmuir 15 (1999) 39 - 43.

[26] L. Qi, H. Co¨lfen, M. Antonietti, Synthesis and Characterization of CdS Nanoparticles Stabilized by Double-Hydrophilic Block Copolymers, Nano Lett. 1 (2001) 61 - 65.

[27] R. Gangopadhyay, A. De, Conducting Polymer Nanocomposites: A Brief Overview, Chem. Mater. 12 (2000) 608 - 622.

[28] Y. Yang, H. Chen, X. Bao, Synthesis and optical properties of CdS semiconductor nanocrystallites encapsulated in a poly (ethylene oxide) matrix, J. Cryst. Growth 252 (2003) 251 - 256.

[29] G. Carrot, S.M. Scholz, C.J.G. Plummer, J.G. Hilborn, J.L. Hedrick, Synthesis and Characterization of Nanoscopic Entities Based on Poly(caprolactone)-Grafted Cadmium Sulfide Nanoparticles, Chem. Mater. 11 (1999) 3571 - 3577.

[30] B. Suo, X. Su, J. Wu, D. Chen, A. Wang, Z. Guo, Poly (vinyl alcohol) thin film filled with CdSe–ZnS quantum dots: Fabrication, characterization and optical properties, Mater. Chem. Phys. 119 (2010) 237–242.

[31] H. Wang, P. Fang, Z. Chen, S. Wang, Synthesis and characterization of CdS/PVA nanocomposite films, Appl. Surf. Scie. 253 (2007) 8495–8499.

[32] X-F. Qian, J. Yin, J-C. Huang, Y-F. Yang, X-X. Guo, Z-K. Zhu, The preparation and characterization of PVA/Ag_2S nanocomposite, Mater. Chem. Phys. 68 (2001) 95–97.

[33] H. Yang, S. Xu, L. Jiang, Y. Dan, Thermal Decomposition Behavior of Poly (Vinyl Alcohol) with Different Hydroxyl Content J. Macromolecular Scie, Part B: Physics 51 (2012) 464–480.

[34] B.J Holland, J.N Hay, The thermal degradation of poly(vinyl alcohol), Polymer 42 (2001) 6775 - 6783.

[35] J. Kuljanin, M.I. Cˇomor, V. Djokovic´, J.M. Nedeljkovic, Synthesis and characterization of nanocomposite of polyvinyl alcohol and lead sulfide nanoparticles, Mater. Chem. Phys. 95 (2006) 67–71.

[36] J. Kuljanin-Jakovljević, M. Marinović-Cincović, Z. Stojanović, A. Krklješ, N.D. Abazović, M.I. Čomor, Thermal degradation kinetics of polystyrene/cadmium sulfide composites, Polymer Degrad. Stab. 94 (2009) 891–897.

[37] S.M. Pawde, K. Deshmukh, Characterization of poly(vinyl alcohol)/gelatin blend hydrogel films for biomedical applications, J. Appl. Polym. Sci. 109 (2008) 3431-3437.

[38] X.F. Qian, J. Yin, J.C. Huang, X.X. Yang, Y.F. Guo, Z.K. Zhu, The preparation and characterization of PVA/Ag2S nanocomposite, Mater. Chem. Phys. 68 (2001) 95 - 97.

[39] J. C. Bruce, N. Revaprasadu, K. R. Koch, Cadmium(II) complexes of N,N-diethyl-N0-benzoylthio(seleno)urea as single-source precursors for the preparation of CdS and CdSe nanoparticles, New J. Chem. 31 (2007) 1647–1653.

[40] N. Moloto, N. Revaprasadu, M.J. Moloto, P. O'Brien, J. Raftery, N,N'-diisopropylthiourea and N,N'-dicyclohexylthiourea zinc(II) complexes as precursors for the synthesis of ZnS nanoparticles, S. Afr. J. Sci. 105 (2009) 258 - 263.

SUPPLEMENTARY FIGURES

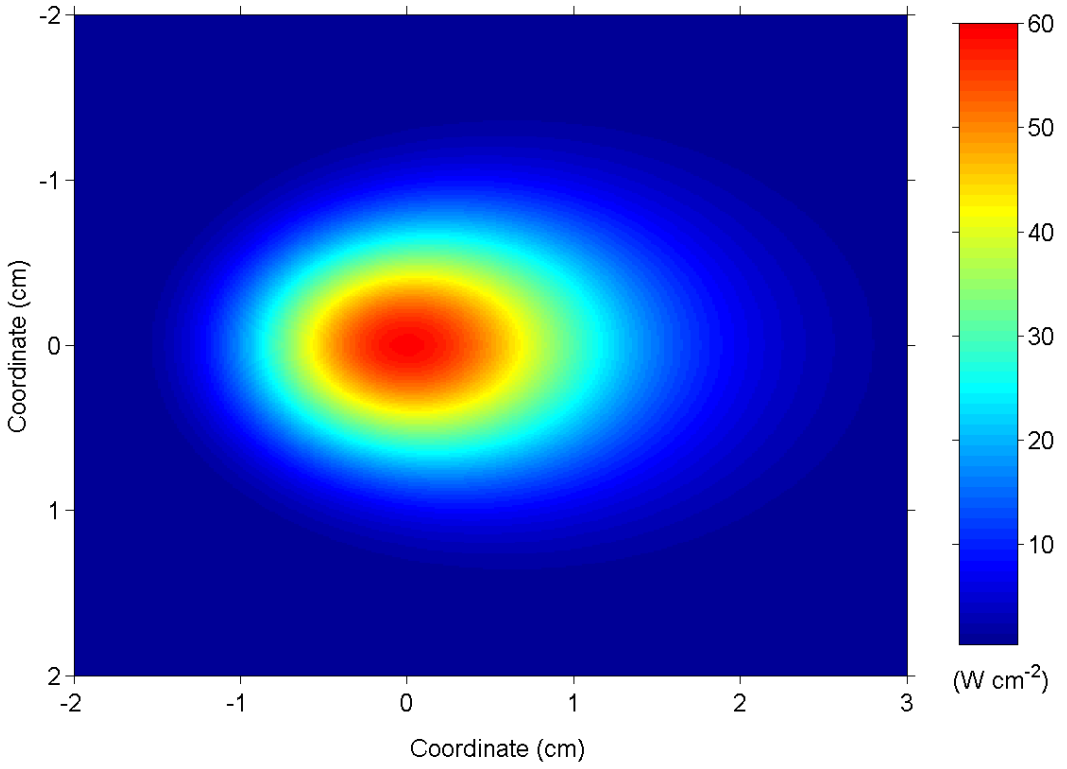

Figure S1: Intensity profile on the substrate surface. The spot size is approximately 32 mm x 20 mm, considering the periphery as the position where the intensity has decreased to e^{-2} for a Gaussian beam approximation.

Figure S2: Substrate samples (a) before irradiation and (b) after irradiation